Center of Excellence for HPC
Astrophysical Applications

4th-Order Accurate Methods for Relativistic MHD with Finite Conductivity

A. Mignone[1], V. Berta[1], M. Bugli[1], G. Mattia[2], M. Rossazza[1], L. Del Zanna[2]

[1]Physics Department, University of Torino (UNITO)

[2]Dipartimento di Fisica e Astronomia – Università di Firenze e INFN – Florence

Co-funded by the European Union

Funded by the European Union. This work has received funding from the European High Performance Computing Joint Undertaking (JU) and Belgium, Czech Republic, France, Germany, Greece, Italy, Norway, and Spain under grant agreement No 101093441.

EuroHPC Joint Undertaking

Outline

- Astrophysical Context;
- Model Equations & Numerical Approach (Finite Volume, 2^{nd} vs 4^{th} order);
- Applications to Magnetic reconnection with effective resistivity;
- Conclusions.

Astrophysical Context

Jets from Active Galactic Nuclei (AGN)

- Powerful jets are produced in the central regions of (some) radio-loud Active Galactic Nuclei (AGN);
- Characterized by non-thermal emission from the radio to the X-rays and γ bands;
- Extends from a few Kpc to some Mpc;

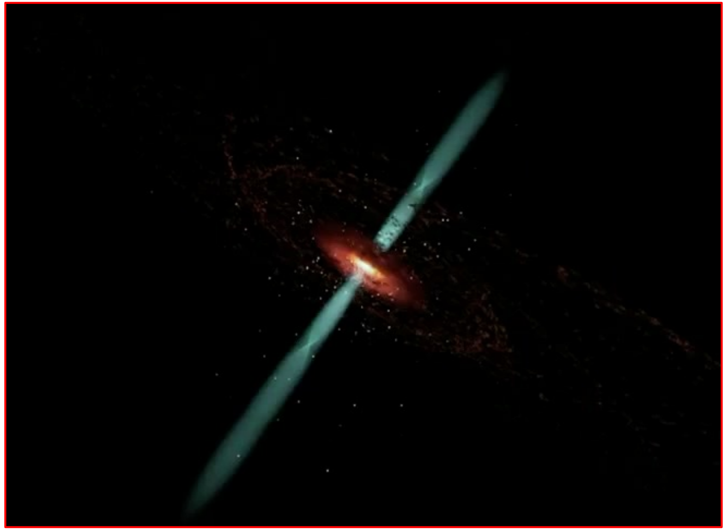

- Convincing evidence of supersonic relativistic flows propagating in partially ordered magnetic fields.

Observations of AGN Jets

- Direct observations of radio-galaxies:
  - radio luminosity that is 10^{39} - 10^{44} ergs/s;
  - Polarization degree 1% - 30%;
  - size from a few kpc to some Mpc;
  - the morphological brightness distribution
  - polarization degree of the radio emission.

- By indirect means:
  - life timescale, 10^7 - 10^8 yrs
  - mean magnetic field, 10 – 10^3 μG,
  - kinetic power, 10^{42} - 10^{47} ergs/s.

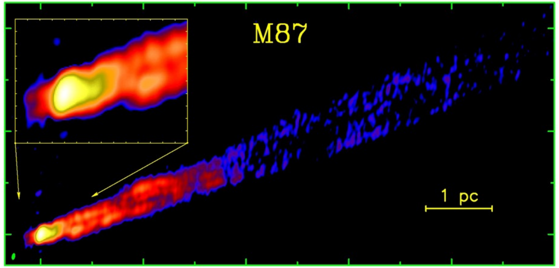

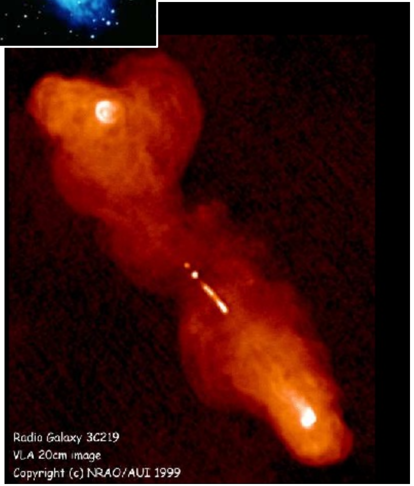

- The values of the jet main physical parameters, such as jet velocity, density and composition, are still under debate after many decades of investigations.

AGN Jets: Emission

- Spectral energy distribution (SED) features two broad humps:

lower energy peak (mm-UV band)
→ synchrotron emission

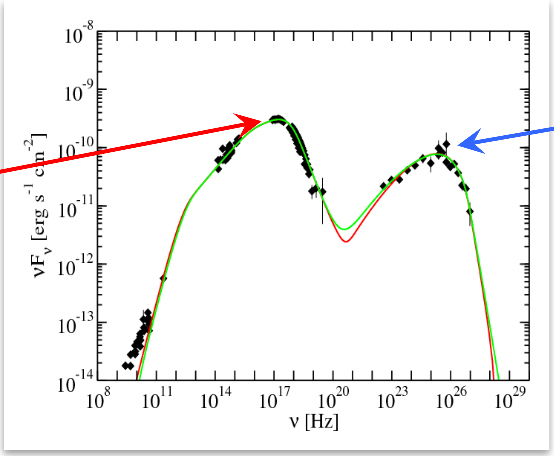

higher energy peak (X- and γ-rays)
→ inverse Compton scattering.

- Strong variability on timescales ≲ day → very compact emission regions where a sizeable fraction of the jet energy flux must be dissipated.
- Part of this energy becomes available to accelerate particles to ultra-relativistic energies.

Dissipation at the Small Scales

Zooming at smaller scales, dissipation mechanisms may operate such as

- ***Collisionless relativistic shocks:*** dissipate kinetic energy into heat very efficiently.
  - prominent sites for particle acceleration through Fermi 1st order process.
  - Efficiency limited to almost ‖ field geometries or weakly magnetized flows[1];

- ***Relativistic magnetic reconnection:*** more promising candidate for producing high-energy particles and powering jet emission at small-scales[2].

- ***Velocity Shear***: particles can gain energy by scattering off small-scale magnetic field irregularities within the turbulent velocity layer at the jet / ambient interface[3].

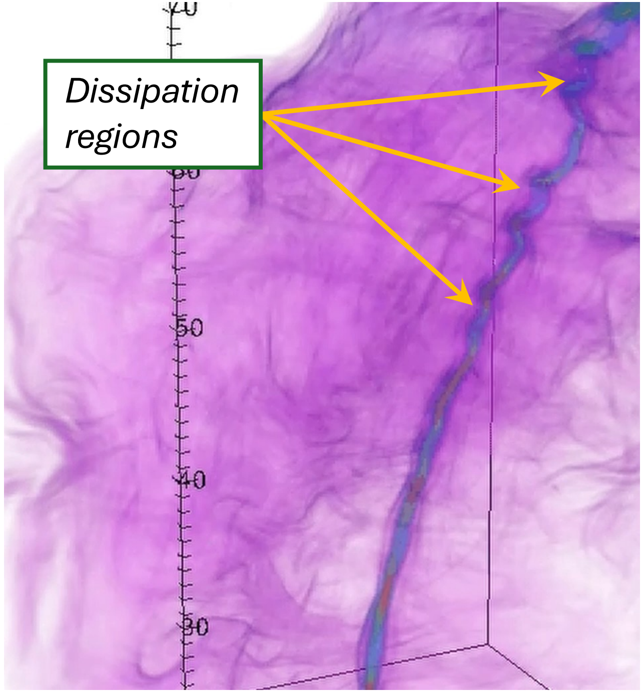

[1]Sironi & Spitkovsky 2009, 2011; [2]Giannios 2013, Sironi & Spitkovsky 2014; [3]Alves et al. 2014

Model Equations & Numerical Approach

Equation Model: Resistive Relativistic MHD

- For $\eta \neq 0$, the equations of (resistive) relativistic MHD (ResRMHD) derived from baryon number conservation, total momentum-energy conservation and Maxwell's equations (Ampere's law):

$$\boxed{\begin{aligned} &\nabla_\mu(\rho \mathbf{u}^\mu) = 0\,, \quad \nabla_\mu\left(T_g^{\mu\nu} + T_{EM}^{\mu\nu}\right) = 0 \\ &\nabla_\mu F^{\mu\nu} = -J^\nu\,, \quad \nabla_\mu F^{*\mu\nu} = 0 \end{aligned}} \longrightarrow \boxed{\begin{aligned} &\frac{\partial D}{\partial t} + \nabla\cdot(D\boldsymbol{v}) = 0, \\ &\frac{\partial \boldsymbol{m}}{\partial t} + \nabla\cdot(w\boldsymbol{u}\boldsymbol{u} + p\mathsf{I} + \mathsf{T}) = 0, \\ &\frac{\partial \mathcal{E}}{\partial t} + \nabla\cdot\boldsymbol{m} = 0, \\ &\frac{\partial \boldsymbol{B}}{\partial t} + \nabla\times\boldsymbol{E} = 0, \\ &\frac{\partial \boldsymbol{E}}{\partial t} - \nabla\times\boldsymbol{B} = -\boldsymbol{J}, \end{aligned}}$$

where

$D = \gamma\rho$	*Mass density*
$\mathcal{E} = w\gamma^2 - p + \mathcal{P}_{\rm EM}$	*Energy Density*
$\boldsymbol{m} = w\gamma\boldsymbol{u} + \boldsymbol{E}\times\boldsymbol{B}$,	*Momentum Density*
$\mathsf{T} = -\boldsymbol{E}\boldsymbol{E} - \boldsymbol{B}\boldsymbol{B} + \frac{1}{2}(E^2 + B^2)\mathsf{I}$	*Maxwell Stress*
$\boldsymbol{J} = \frac{1}{\eta}[\gamma\boldsymbol{E} + \boldsymbol{u}\times\boldsymbol{B} - (\boldsymbol{E}\cdot\boldsymbol{u})\boldsymbol{v}] + q\boldsymbol{v}$	*Current Density* [J'= σ E']
$\nabla\cdot\boldsymbol{B} = 0, \quad \nabla\cdot\boldsymbol{E} = q$	*Constraints*

Equation Model: Resistive Relativistic MHD

- ResRMHD eqns admits 10 propagating modes*, easily recognized in the small/large conductivity limits:

  - for η → ∞, matter and EM fields decouple; solution modes → pairs of light and acoustic waves (+ purely damped modes);

  - for η → 0 (ideal) limit, modes → pair of fast magnetosonic / slow / Alfvén modes. The contact mode unaffected by the conductivity.

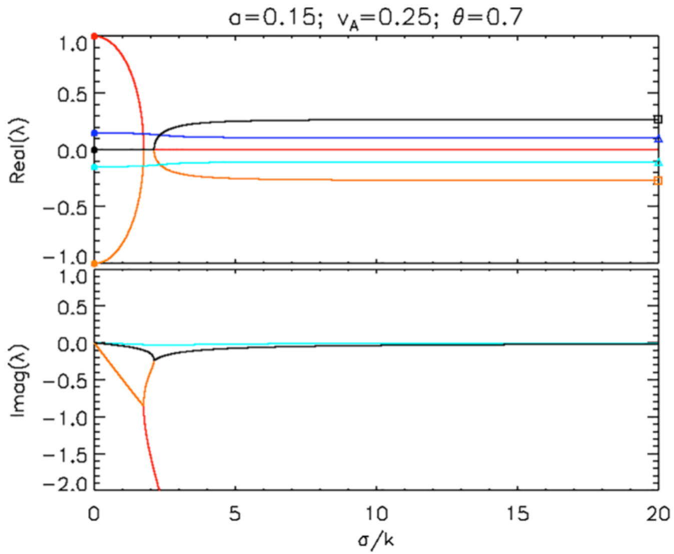

! Important: resistivity is *collisional* in origin: $$\eta = \frac{c^2}{4\pi\sigma}\,, \qquad \text{where} \quad \sigma = \frac{e^2 n_e}{m_e \nu_{ep}}$$

[*] Mignone, Mattia & Bodo, Phys. Plasma 25, 092114 (2018)

Numerical method: Finite Volume Formulation

- We employ finite volume, so that integrating the previous differential equations over a control volume, yields (for zone-centered variables):

$$\frac{\partial U}{\partial t} = -\nabla\cdot F + S \quad\Longrightarrow\quad \frac{d\langle U\rangle}{dt} = -\oint F\cdot dS + \frac{1}{\Delta V}\int S dV$$

where

$$-\left(\frac{\hat{F}_{x,\mathbf{x}_f} - \hat{F}_{x,\mathbf{x}_f-\hat{\mathbf{e}}_x}}{\Delta x} + \frac{\hat{F}_{y,\mathbf{y}_f} - \hat{F}_{y,\mathbf{y}_f-\hat{\mathbf{e}}_y}}{\Delta y} + \frac{\hat{F}_{z,\mathbf{z}_f} - \hat{F}_{z,\mathbf{z}_f-\hat{\mathbf{e}}_z}}{\Delta z}\right)$$

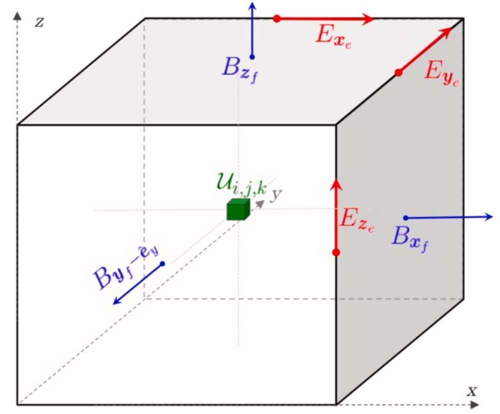

$$\langle U\rangle_c \equiv \frac{1}{\Delta x\Delta y\Delta z}\int U(x,y,z,t)\,dx\,dy\,dz\,,$$

$$\hat{F}_{x,\mathbf{x}_f} \equiv \frac{1}{\Delta y\Delta z}\int \hat{\mathbf{e}}_x\cdot \mathsf{F}\big(U(x_{i+\frac{1}{2}},y,z,t)\big)\,dy\,dz\,,$$
$$\hat{F}_{y,\mathbf{y}_f} \equiv \frac{1}{\Delta x\Delta z}\int \hat{\mathbf{e}}_y\cdot \mathsf{F}\big(U(x,y_{j+\frac{1}{2}},z,t)\big)\,dz\,dx\,,$$
$$\hat{F}_{z,\mathbf{z}_f} \equiv \frac{1}{\Delta x\Delta y}\int \hat{\mathbf{e}}_z\cdot \mathsf{F}\big(U(x,y,z_{k+\frac{1}{2}},t)\big)\,dx\,dy\,.$$

and $U=(D, m, \mathcal{E}, \mathbf{E})$ is an array of conserved variables

- This is called the *integral form* of the equations.

Finite Volume + Constrained Transport

- Magnetic fields retains a staggered representation (face-centered) and it is evolved through a discrete version of the Stokes theorem,

$$
\begin{aligned}
\frac{d\hat{B}_{x,\mathbf{x}_f}}{dt} &= -\left(\frac{\bar{E}_{z,\mathbf{z}_e}-\bar{E}_{z,\mathbf{z}_e-\hat{\mathbf{e}}_y}}{\Delta y}-\frac{\bar{E}_{y,\mathbf{y}_e}-\bar{E}_{y,\mathbf{y}_e-\hat{\mathbf{e}}_z}}{\Delta z}\right)\\
\frac{d\hat{B}_{y,\mathbf{y}_f}}{dt} &= -\left(\frac{\bar{E}_{x,\mathbf{x}_e}-\bar{E}_{x,\mathbf{x}_e-\hat{\mathbf{e}}_z}}{\Delta z}-\frac{\bar{E}_{z,\mathbf{z}_e}-\bar{E}_{z,\mathbf{z}_e-\hat{\mathbf{e}}_x}}{\Delta x}\right)\\
\frac{d\hat{B}_{z,\mathbf{z}_f}}{dt} &= -\left(\frac{\bar{E}_{y,\mathbf{y}_e}-\bar{E}_{y,\mathbf{y}_e-\hat{\mathbf{e}}_x}}{\Delta x}-\frac{\bar{E}_{x,\mathbf{x}_e}-\bar{E}_{x,\mathbf{x}_e-\hat{\mathbf{e}}_y}}{\Delta y}\right)
\end{aligned}
$$

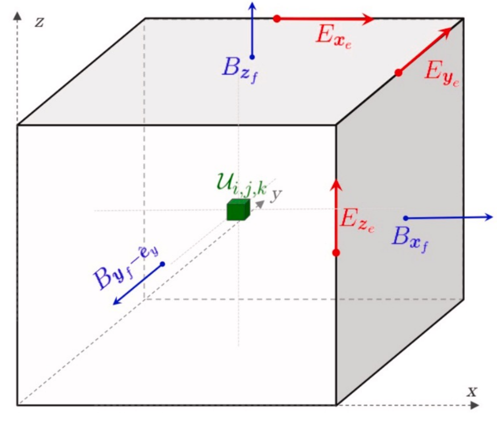

where, e.g. $$\hat{B}_{x,x_f} = \frac{1}{\Delta y \Delta z}\int \mathbf{B}(x_{i+\frac{1}{2}}, y_j, z_k)\cdot d\mathbf{S}_x$$

$$
\begin{aligned}
\bar{E}_{x,\mathbf{x}_e} &\equiv \frac{1}{\Delta x}\int E_x(x, y_{j+\frac{1}{2}}, z_{k+\frac{1}{2}}, t)\,dx\,,\\
\bar{E}_{y,\mathbf{y}_e} &\equiv \frac{1}{\Delta y}\int E_y(x_{i+\frac{1}{2}}, y, z_{k+\frac{1}{2}}, t)\,dy\,,\\
\bar{E}_{z,\mathbf{z}_e} &\equiv \frac{1}{\Delta z}\int E_z(x_{i+\frac{1}{2}}, y_{j+\frac{1}{2}}, z, t)\,dz\,.
\end{aligned}
$$

- This ensure that $\nabla\cdot B=0$ condition is respected to machine accuracy.

Flux Computation → Riemann Solver

- In 1D →

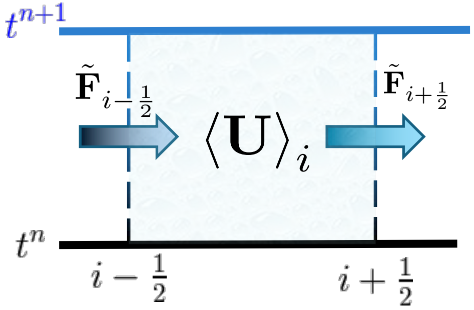

- Fluxes computed by solving the so-called “*Riemann Problem*”, i.e., the evolution of a discontinuity separating two *constant* states:

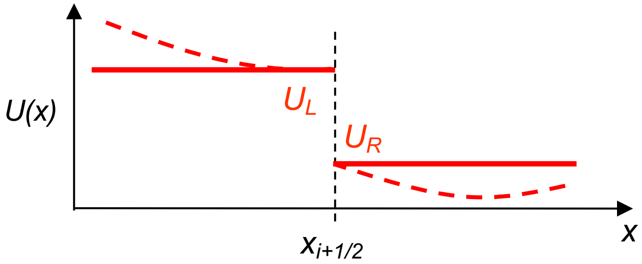

$$\boxed{U(x,0) = \begin{cases} U_L & \text{for} \quad x < x_{i+\frac{1}{2}} \\ U_R & \text{for} \quad x > x_{i+\frac{1}{2}} \end{cases} \quad \Longrightarrow \quad U(x_{i+\frac{1}{2}}, t>0) = ?}$$

- Solution always considered to be discontinuous at cell interfaces: different level of approximation can be used*.

[*] Mignone et al, MNRAS, 486, 4252-4274 (2019)

Extension to 4^{th}-Order Method

- We draw on the original formulation by McCorquodale & Colella (2011)* and **.

- Volume average and point value interchangeable only at 2^{nd} order: $\langle U \rangle_c - U_c = O(h^2)$

- To 4^{th} order, e.g. $\boxed{U_c = \left(1 - \frac{\Delta}{24}\right) \langle U \rangle_c + O(h^4)}$ with $\Delta \langle U \rangle_c \equiv (\Delta^x + \Delta^y + \Delta^z) \langle U \rangle_c$

- "De-averaging" using Laplacian operators: $\Delta^x \langle U \rangle_c = \left(\langle U \rangle_{c-\hat{e}_x} - 2 \langle U \rangle_c + \langle U \rangle_{c+\hat{e}_x}\right)$

- Averaging follows the inverse rule, e.g. $\boxed{\hat{F}_{x,\mathbf{x}_f} = F_{x,\mathbf{x}_f} + \frac{\Delta_\perp^x F_{x,\mathbf{x}_f}}{24}}$ $\boxed{\bar{E}_{z,\mathbf{z}_e} = \left(1 + \frac{\Delta^z}{24}\right) E_{z,\mathbf{z}_e}}$

- In its simplest form, a 4^{th} - order scheme can be designed by retaining the typical dimension by dimension strategy while relying on 1D operators.

[*]McCorquodale & Colella, Commun. Appl. Math. Comput. Sci. 6(1): 1-25 (2011) [**]Felker & Stone , JCP 375, 1365 (2019)

Time Stepping: Handling Stiffness

- Time evolution based on semi-discrete approach (method of lines), with stiff source ($\eta \ll 1$) term

$$\frac{d\left\langle U\right\rangle_c}{dt} = -\oint \mathbf{F}\cdot d\mathbf{A} + \left\langle S\right\rangle_c \equiv R + S$$

$$\begin{aligned}
\frac{\partial D}{\partial t} + \nabla\cdot(D\boldsymbol{v}) &= 0, \\
\frac{\partial \boldsymbol{m}}{\partial t} + \nabla\cdot(w\boldsymbol{u}\boldsymbol{u} + p\mathsf{I} + \mathsf{T}) &= 0, \\
\frac{\partial \mathcal{E}}{\partial t} + \nabla\cdot\boldsymbol{m} &= 0, \\
\frac{\partial \boldsymbol{B}}{\partial t} + \nabla\times\boldsymbol{E} &= 0, \\
\frac{\partial \mathbf{E}}{\partial t} - \nabla\times\mathbf{B} &= -\mathbf{J} \equiv -\frac{\tilde{\mathbf{E}}}{\eta}
\end{aligned}$$

- → IMplicit-Explicit (IMEX) RK methods*:

IMEX-SSP3(4,3,3) L-stable [*]

$$\langle U\rangle_c^{(k)} = \langle U\rangle_c^n + \Delta t\sum_{j=1}^{k-1}\tilde{a}_{kj}\hat{R}_c + \Delta t\sum_{j=1}^{k} a_{kj}\,\langle S\rangle_c^{(j)},$$

$$\langle U\rangle_c^{n+1} = \langle U\rangle_c^n + \Delta t\sum_{j=1}^{\nu}\tilde{w}_j\hat{R}_c^{(j)} + \Delta t\sum_{j=1}^{\nu} w_j\,\langle S\rangle_c^{(j)},$$

Butcher Tableaux for SSP3(4,3,3):

$$\begin{array}{c|cccc}
0 & 0 & 0 & 0 & 0 \\
0 & 0 & 0 & 0 & 0 \\
1 & 0 & 1 & 0 & 0 \\
1/2 & 0 & 1/4 & 1/4 & 0 \\
\hline
 & 0 & 1/6 & 1/6 & 2/3
\end{array}
\qquad
\begin{array}{c|cccc}
\alpha & \alpha & 0 & 0 & 0 \\
0 & -\alpha & \alpha & 0 & 0 \\
1 & 0 & 1-\alpha & \alpha & 0 \\
1/2 & \beta & \eta & 1/2-\beta-\eta-\alpha & \alpha \\
\hline
 & 0 & 1/6 & 1/6 & 2/3
\end{array}$$

[*] Pareschi L., Russo G., 2005, Journal of Scientific Computing, 25, 129

Accuracy Assessment: CP Alfvén Waves

- Circularly polarized Alfvén waves on $[0,1]^3$, $\begin{pmatrix} v_x \\ v_y \\ v_z \end{pmatrix} = \begin{pmatrix} 0 \\ -c_A\eta\cos\phi \\ -c_A\eta\sin\phi \end{pmatrix}$, $\begin{pmatrix} B_x \\ B_y \\ B_z \end{pmatrix} = \begin{pmatrix} B_0 \\ B_0\eta\cos\phi \\ B_0\eta\sin\phi \end{pmatrix}$ $\quad \phi = \mathbf{k}'\cdot\mathbf{x}' - \omega t$

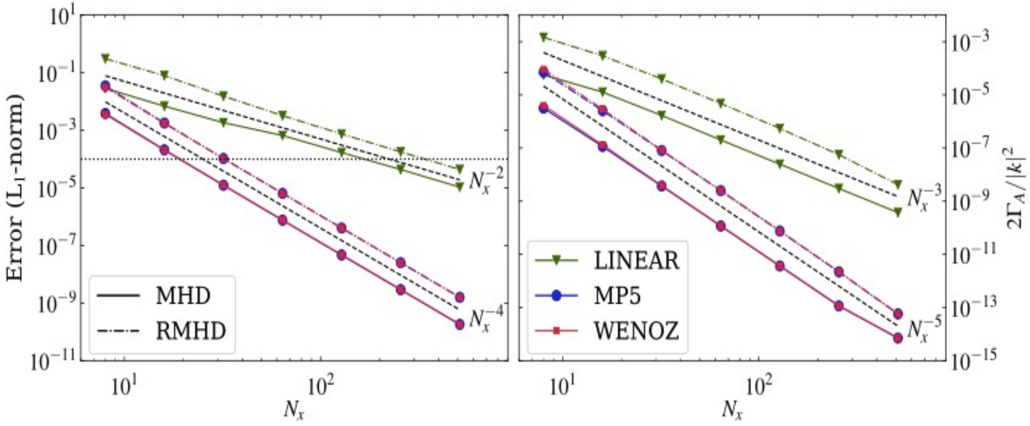

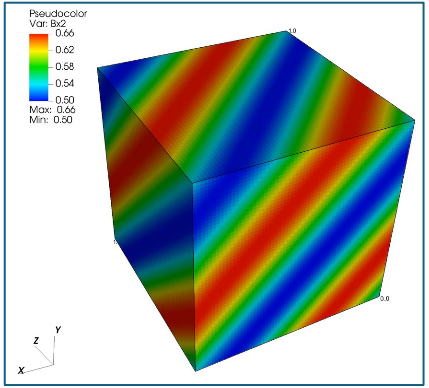

CPU time saving: for 2nd and 4th order to achieve the same accuracy, N_2 and N_4 are related by

$$N_4 \sim \left(\frac{C_4}{C_2}\right)^{1/4}\sqrt{N_2} \quad \rightarrow \quad \text{in terms of CPU time} \quad \rightarrow \quad \frac{T_4}{T_2} = \left(\frac{C_4}{C_2}\right)^{(d+1)/4}\frac{\tau_4}{\tau_2}\frac{1}{\sqrt{N_2^{d+1}}}$$

$C_4/C_2 \sim \{5, 8.7\}$, $\tau_4/\tau_2 \sim \{4.3, 3.7\}$ → $\boxed{T_4/T_2 \sim K/N_2^2 \ \text{with}\ K \sim \{21, 32\}}$

[*] Berta et al., JCP., 499, 112701 (2024); [**] Mignone et al, MNRAS (accepted)

Application to Relativistic Reconnection: Ideal Tearing Mode

- Ideal tearing mode in *ResRMHD*, with FF equilibrium

$$\mathbf{B} = B_0 \left[\tanh\left(\frac{x}{a}\right)\hat{\mathbf{e}}_y + \mathrm{sech}\left(\frac{x}{a}\right)\hat{\mathbf{e}}_z\right] \qquad S = v_a L/\eta$$

- For sufficiently thin CS, $a = S^{-1/3}L$ → the reconnection process occurs on the ideal Alfvénic time scale: $\tau_a = L/v_a$

- In the limit of large S → *ideal* tearing instability [*],[**]

- Linear growth converges faster for 4^{th} order scheme

  → $N_4 \lesssim N_2/2$

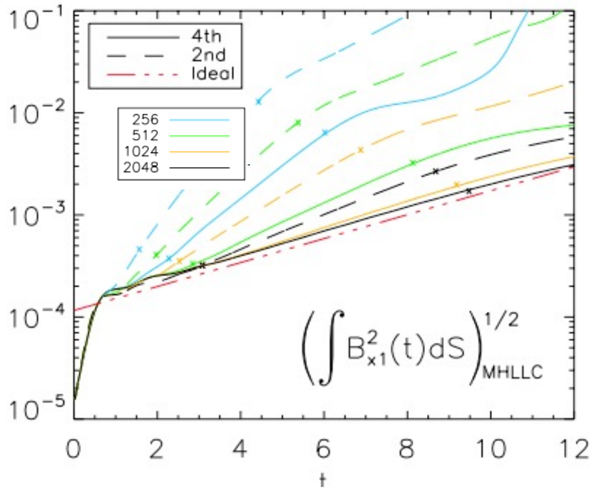

Resolution	2^{nd}-order	4^{th}-order
256×64	1.19	0.75
512×128	0.89	0.44
1024×256	0.58	0.30
2048×512	0.38	0.27

Collisionless Effective Resistivity

Collisionless Resistivity: 2D PIC Models

- Selvi et al.[1] (2023) analyzed 2D current sheets with PIC simulations of pair plasmas;

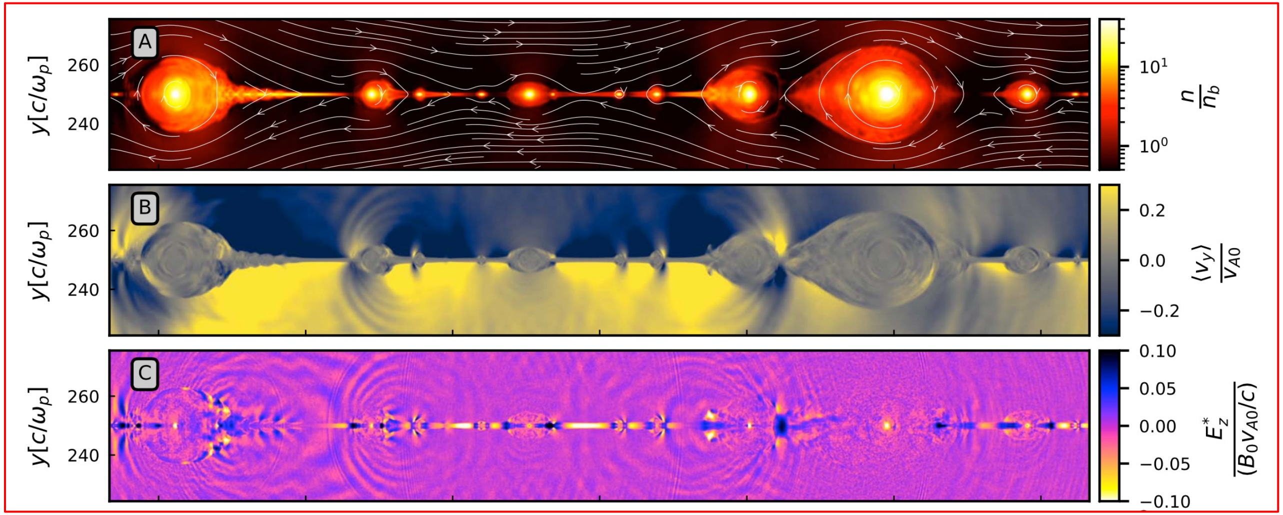

- At X-points, diverging flows result in a nondiagonal thermal pressure tensor: finite residence time for particles gives rise to a localized *collisionless effective resistivity.*

Effective Resistivity from PIC 2D Models

→ Statistical analysis of Ohm's law to identify nonideal electric field contributions. Each species *s=e,p* (e.g. electron/positron) contributes:

$$\boldsymbol{E} = -\frac{\langle \boldsymbol{v}_t \rangle}{c} \times \boldsymbol{B} + \sum_s \frac{\rho_s}{n_t e_s} \left[\partial_t \langle \boldsymbol{u}_s \rangle + \langle \boldsymbol{v}_s \rangle \cdot \nabla \langle \boldsymbol{u}_s \rangle \right] + \sum_s \frac{1}{n_t e_s} \nabla \cdot \mathcal{P}_s$$

$$\boldsymbol{E} = [\text{ideal}] + [\text{temporal}] + [\text{convective}] + [\text{thermal}]$$

n_t	$=$	$n_e + n_p$	Total number density
$\boldsymbol{u}_s$	$=$	$\gamma_s \boldsymbol{v}_s$	Four Velocity
$\mathcal{T}_s$	$=$	$\rho_s \langle \boldsymbol{u}_s \boldsymbol{v}_s \rangle$	Total energy − mom. tensor
$\mathcal{P}_s$	$=$	$\mathcal{T}_s - \rho_s \langle \boldsymbol{v}_s \rangle \langle \boldsymbol{u}_s \rangle$	Thermal pressure tensor

ram pressure tensor

- Dominant contribution given by non-gyrotropic thermal pressure term.

The Non-Ideal Electric Field at an X-point

Non-ideal E dominated by yz-ram pressure term in the reconnection layer (2D PIC, no guide field)

$$+$$

$$e_z = \eta_{\text{eff}} j_z$$

$$\Downarrow$$

$$\eta_{\text{eff}} = \frac{m}{n_t e^2} \frac{\langle u_{s,z} \rangle}{\langle v_{s,z} \rangle} \partial_y \langle v_{s,y} \rangle$$

$$\Downarrow ?$$

$$\eta_{\text{eff}} \simeq \frac{m^2}{\rho e^2} \gamma \partial_y v_y$$

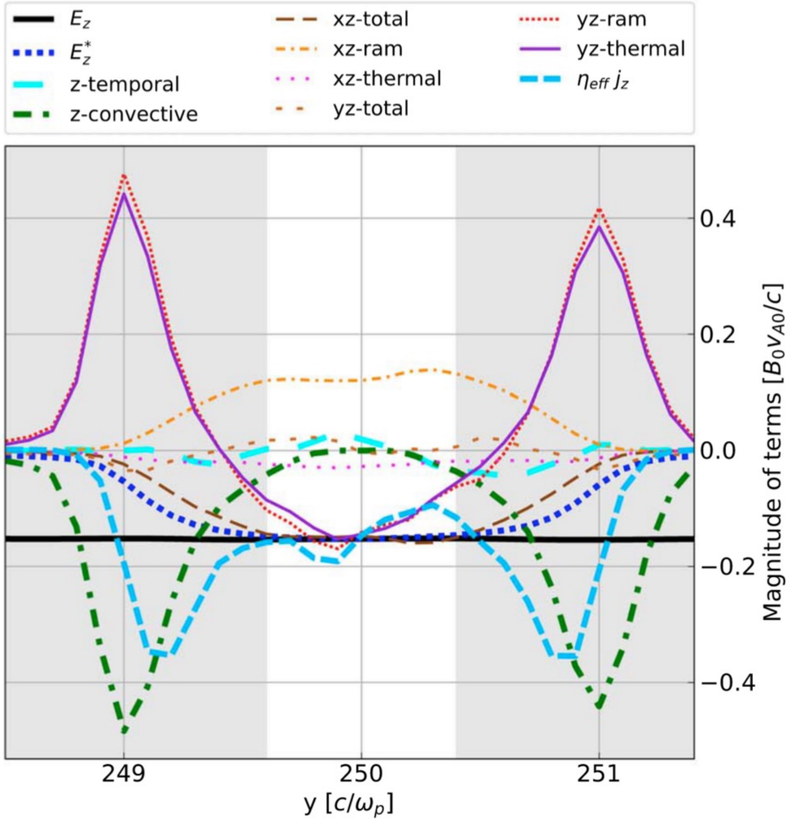

Effective Resistivity in Fluid Model

- Reformulated in terms of the spatial current density in the fluid frame,

$$\eta_{\text{eff}} = \frac{mc\partial_y v_y}{e\sqrt{\left(\frac{\rho e c}{m}\right)^2 - j_z^2}} \Rightarrow \eta_{\text{eff}} = \frac{\sqrt{\left(\frac{mc}{e}\partial_y v_y\right)^2 + e_z^2}}{\frac{\rho e c}{m}}$$

Dimensionless resistivity

$$\boxed{\bar{\eta}_{\text{eff}} = \frac{1}{\bar{\rho}}\frac{\delta_0}{L_0}\sqrt{\bar{e}_z^2 + \left(\frac{\delta_0}{L_0}\right)^2 (\partial_{\bar{y}}\bar{v}_y)^2}}$$

with $\delta_0 = c/\omega_0 = c/\sqrt{\frac{4\pi e^2 \rho_0}{m^2}}$ and L_0, ρ_0 scale quantities.

- $e_z = \gamma(\mathbf{E} + \mathbf{v} \times \mathbf{B})_z$ is the rest-frame electric field.
- Nonuniform nature of the effective resistivity may give a 1st approximation to collisionless reconnection in a (fluid) MHD description;
- No "free" parameters (as in Ripperda et al., 2019b);
- Dissipation is set by problem's scale and plasma properties.

[*] Bugli et al., in prep

Validation: 1D Self-Similar Current Sheet

- Temporal evolution of a 1D current sheet: comparison between effective and constant resistivity:

Constant resistivity

Standard test for Res(G)RMHD codes

$$B_y(x,t) = \mathrm{erf}\left(\frac{x}{2\sqrt{\eta t}}\right) \quad \text{(Komissarov, 2007)}$$

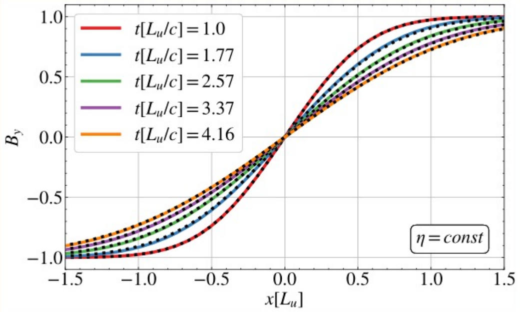

Effective resistivity

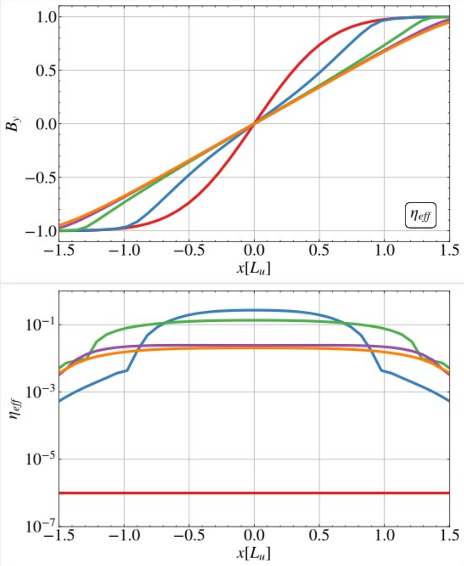

2D Current Sheet with Effective Resistivity

- 2D relativistic MHD models with non-uniform resistivity using both relativistic MHD (PLUTO code) and PIC (ZELTRON code).

- Initial condition:

Harris current sheet (pressure balance)

$$B_x(y) = B_0 \tanh\left(\frac{y}{a}\right), \quad p(y) = \frac{1}{2}B_0^2(\beta_0 + 1) - \frac{1}{2}B_x^2(y).$$

- Parameters:

  - Constant temperature $\rightarrow \rho = \rho_0 p / p_0$
  - $B_0 = \sqrt{\sigma_0 \rho_0}$, $\beta_0 = 0.01$
  - $c_{A,0} = (1/\sigma_0 + 2\beta_0 + 1)^{-1/2}$
  - $(x, y) \in [0, 4L] \times [-80\sqrt{\sigma_0}a, 80\sqrt{\sigma_0}a]$
  - Periodic BC in x, reflective BC in y
  - $L = 1$, $a = 0.01L = \delta_0/2 = 5c/\omega_p$
  - PIC benchmark performed with the ZELTRON code (Cerutti et al., 2013)

2D Current Sheet with Effective Resistivity

- 2D relativistic MHD model with non-uniform resistivity.

Model	σ_0	$c_{A,0}$	$\bar{\eta}$	ρ_0	B_0/ρ_0
s10eEr1	10	0.945	$\eta_{\rm eff}$	1	3.16
s4eEr1	4	0.887	$\eta_{\rm eff}$	1	2
s1eEr1	1	0.704	$\eta_{\rm eff}$	1	1
s10eEr01	10	0.945	$\eta_{\rm eff}$	0.1	10
s10eEr10	10	0.945	$\eta_{\rm eff}$	10	1
s10eC-2r1	10	0.945	2.5×10^{-2}	1	3.16
s10eC-3r1	10	0.945	2.5×10^{-3}	1	3.16
s10eC-4r1	10	0.945	2.5×10^{-4}	1	3.16
s10eC-5r1	10	0.945	2.5×10^{-5}	1	3.16

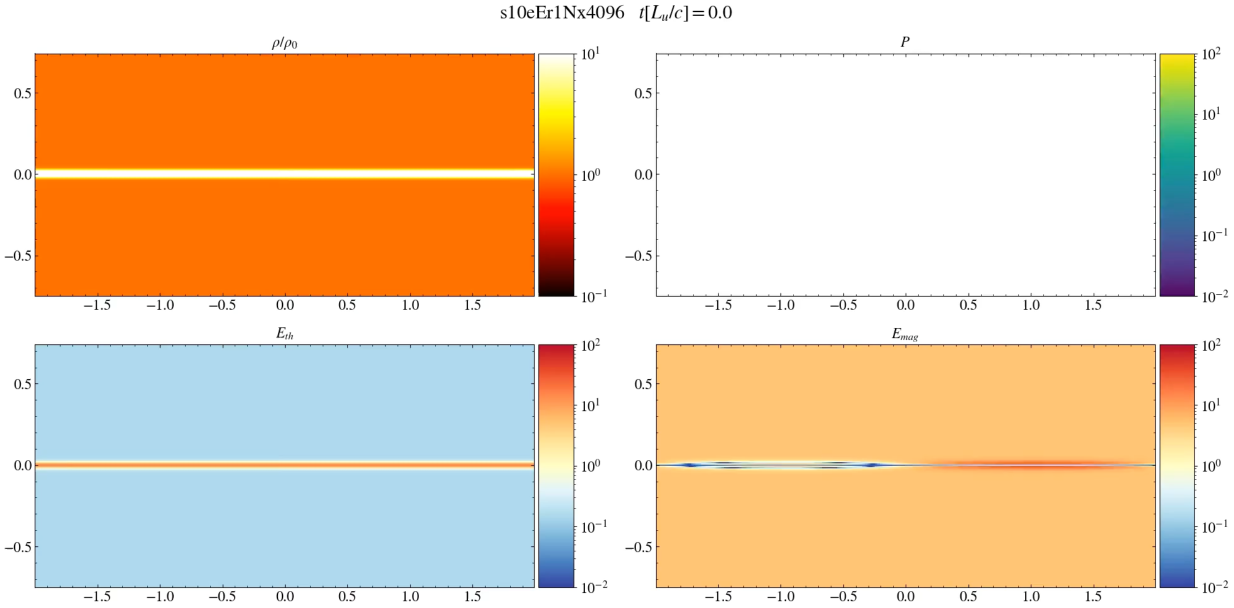

Effective Resistivity Profile

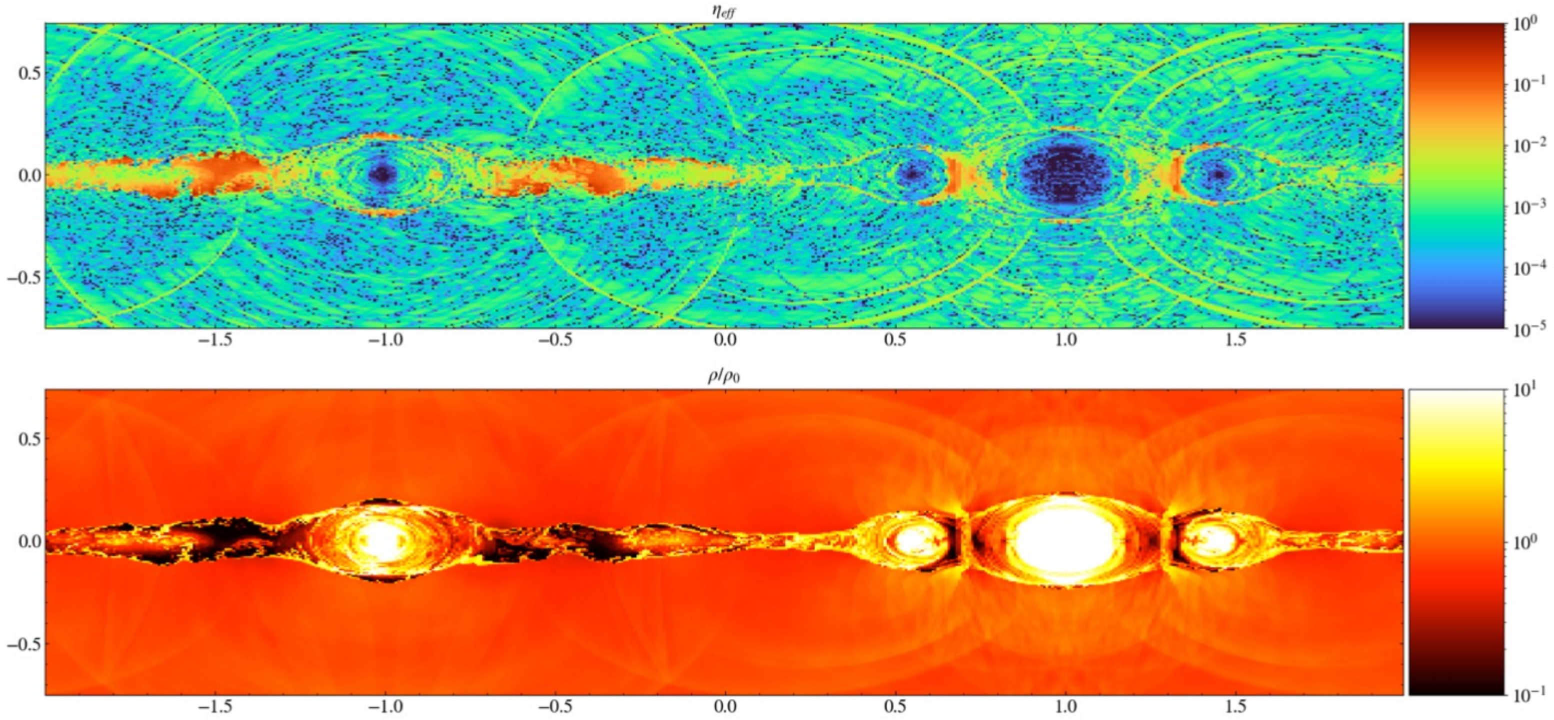

Effective vs. Constant Resistivity

Tearing instability

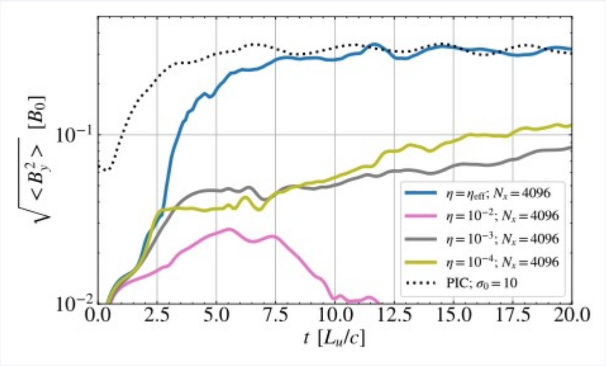

Resistivity

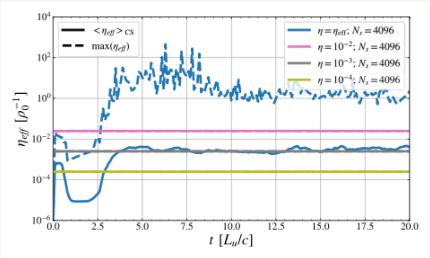

Reconnected flux and rate

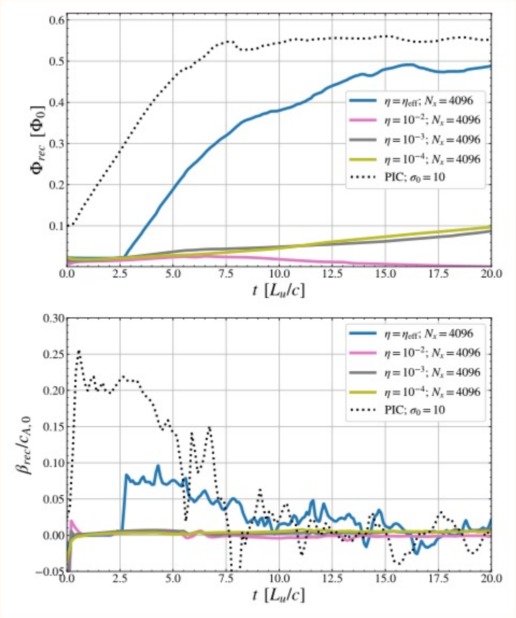

$$\Phi_{\rm rec} = -\int_{x_X}^{x_O} B_y(x,0)dx = A_z\big|_X - A_z\big|_O$$

Dependence on Grid Resolution

- Effective η prescription captures the onset of magnetic reconnection even at low resolutions, $N_x \approx 256$ (models with constant η require generally much higher resolutions to converge).

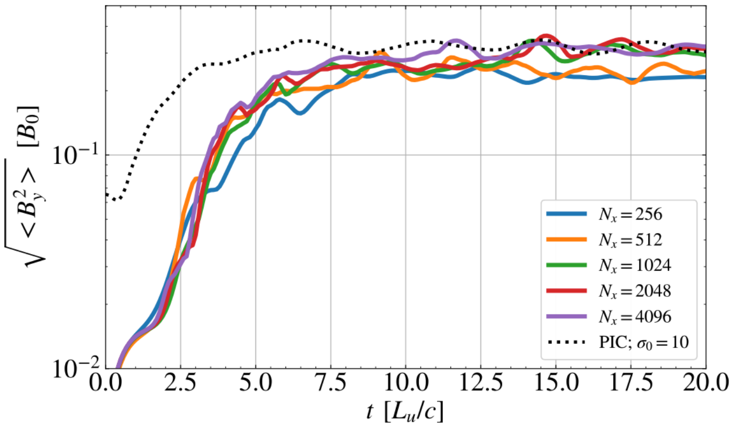

- Reconnecting magnetic fluxes in agreement for $N_x \gtrsim 2048$ by the end of simulation, with the highest resolution case showing a slightly faster and more continuous reconnection.

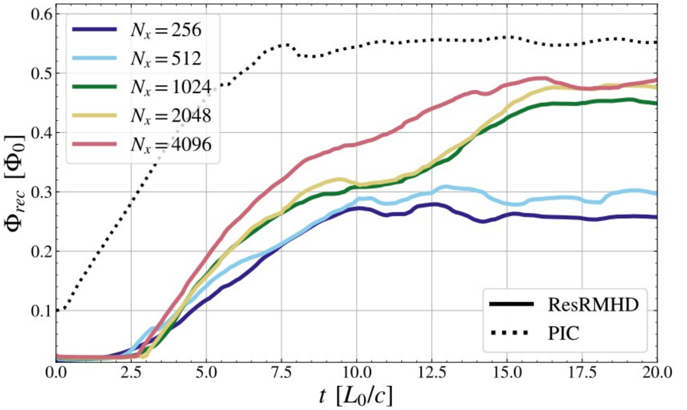

gPLUTO: the next GPU Version of the PLUTO Code

- 4th order method successfully implemented in gPLUTO – the upcoming GPU version of the PLUTO code, developed within the SPACE CoE.

- SPACE (**S**calable **P**arallel **A**strophysical **C**odes for **E**xascale): Center of Excellence funded by the European HPC Joint Undertaking (JU).

- The CoE's primary objective is to prepare 7 of the existing state-of-the-art European HPC astrophysics and cosmology codes for the transition to exa-scale on Euro HPC facilities.

- SPACE involves co-design activities bringing together scientists, code developers, HPC experts, HW manufacturers and SW developers.

Conclusions

- 4th order schemes deliver smaller dissipation, higher accuracy, CPU saving and more efficient computations;

- Non-uniform, effective resistivity model provides a viable opportunity to design physically grounded global models for reconnection-powered high-energy emission.

- Application to 2D reconnection: good agreement between PIC and ResRMHD models with effective resistivity:
  - Strong localization of magnetic dissipation within the current sheet
  - Dissipation set by the system's dynamics and introduction of a characteristic scale δ_0.
  - Good results even at modest resolutions, while constant η case calls for much larger resolutions;

Center of Excellence for HPC
Astrophysical Applications

Thank You

Co-funded by
the European Union

Funded by the European Union. This work has received funding from the European High Performance Computing Joint Undertaking (JU) and Belgium, Czech Republic, France, Germany, Greece, Italy, Norway, and Spain under grant agreement No 101093441.

EuroHPC
Joint Undertaking